PHYSICAL REVIEW A **79**, 011801(R) (2009)

Linearly polarized bistable localized structure in medium-size vertical-cavity surface-emitting lasers

Xavier Hachair,[1] Giovanna Tissoni,[2] Hugo Thienpont,[1] and Krassimir Panajotov[1,3]
[1]*Department of Applied Physics and Photonics (IR-TONA), Vrije Unversiteit Brussels, Pleinlaan 2, B-1050 Brussels, Belgium*
[2]*INFM-CNR and CNISM, Dipartimento di Fisica e Matematica, Università dell'Insubria, Via Valleggio 11, 22100 Como, Italy*
[3]*Institute of Solid State Physics, Tzarigradsko Chaussee Boulevard, 72, Sofia, Bulgaria*
(Received 14 May 2008; revised manuscript received 20 October 2008; published 6 January 2009)

We show that a 40-μm-diameter vertical-cavity surface-emitting laser (VCSEL) is capable of supporting spatially localized structures with linear polarization, orthogonal to the principal polarization. The VCSEL is biased above the lasing threshold and emits a well-defined linear polarization (principal polarization). A holding beam with orthogonal polarization is injected into the cavity, and a localized structure is spontaneously switched on. The orthogonally polarized localized structure is shown to be bistable when the injection current is varied. Numerical results based on a rate equation model support the experimental findings.

DOI: 10.1103/PhysRevA.79.011801 PACS number(s): 42.55.−f, 42.65.Pc, 42.65.Sf, 42.65.Tg

Broad-area vertical-cavity surface-emitting lasers (VCSELs) have recently been a subject of considerable interest due to their potential for applications to all-optical information processing [1,2]. Thanks to the large Fresnel number of broad-area VCSELs, cavity solitons have been experimentally demonstrated in these devices [3].

Cavity solitons (CSs) are localized spots of light in the transverse plane of a broad-area beam transmitted through a nonlinear cavity, which is driven by a homogeneous holding beam (HB). They can be generated spontaneously or by injection into the cavity of a writing or erasing laser pulse [3,4]. So far CSs have been created in broad-area VCSELs (typically with a diameter of 150–200 μm) in order to guarantee independence of the transverse boundaries. These boundary conditions are due not only to the geometrical shape of the device but also to current crowding, i.e., a piling up of injected carriers close to the perimeter of the oxide aperture. For small bias currents, the emission occurs only around the boundaries of the device with a "ring" or "flower" mode profile, clearly reflecting the boundary determined nature of the emission [5]. As the bias current is increased, the laser emission fills in progressively the whole transverse plane; however, no transition from bound to spontaneous patterns takes place [5,6]. Such a "bounded" laser emission in a single high-order mode or a combination of several such modes prevents the existence of localized structures. However, it actually brings to life, as we will demonstrate in the following, spontaneous patterns and localized structures in the nonlasing, orthogonal linear polarization.

Indeed, VCSELs exhibit peculiar polarization behavior. Small-area devices emit linearly polarized (LP) light when operating in the fundamental mode; however, the polarization may switch between two orthogonal directions as current or temperature is changed [7,8]. Such polarization switching has been extensively studied also for the cases of optical feedback [9,10] and optical injection [11,12] in small-area VCSELs. In contrast, polarization dynamics in broad-area VCSELs are not yet that well investigated and understood, although some recent studies on polarized patterns have been carried out. It has been demonstrated that, as in small-area VCSELs, one linear polarization can be predominant ("principal" polarization) close to the lasing threshold while its orthogonal polarization is strongly suppressed [13,14].

In this paper, we experimentally demonstrate the possibility of creating a pattern and a bistable localized structure in the orthogonal polarization without influencing the principal one. With this aim we apply the orthogonal holding beam, i.e., the polarization of the holding beam is linearly polarized but orthogonal to the principal polarization of the VCSEL. Furthermore, we show that by using this method one can substantially reduce the impact of the current crowding.

Our experimental setup is schematically shown in Fig. 1. We use a commercial GaAs quantum well VCSEL emitting around 850 nm with a circular oxide aperture with a diameter of 40 μm. The master laser, which provides the holding beam, is an external-grating semiconductor laser (TEC 100 of Sacher Lasertechnik) that can be tuned in the range of 845–855 nm. The holding beam is spatially filtered and prepared by an optical system (SF) to obtain a collimated beam with a waist of 60 μm. Its intensity can be considered almost constant across the cross section of the VCSEL. The master laser is isolated from the VCSEL by an optical isolator (OFR IO-5-TiS2-HP). The orientation of the LP holding beam can be turned by a half-wave plate. The power of the injection beam entering the VCSEL through the collimator is 8 mW.

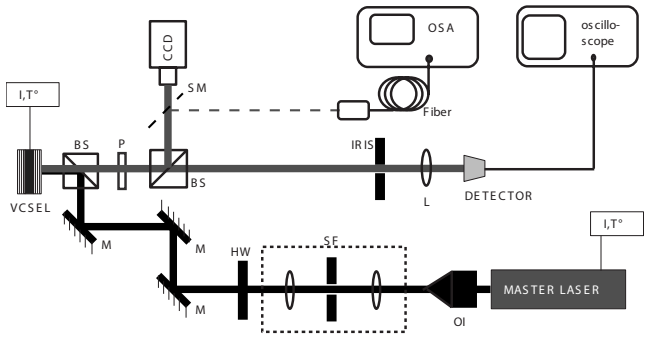

FIG. 1. Experimental setup. BS, beamsplitter; M, mirror; L, lens; OI, optical isolator; P, polarizer; I,T-current (I) driver and temperature (T) controller; SM, semitransparent mirror; SF, spatial filter; OSA, optical spectrum analyzer.

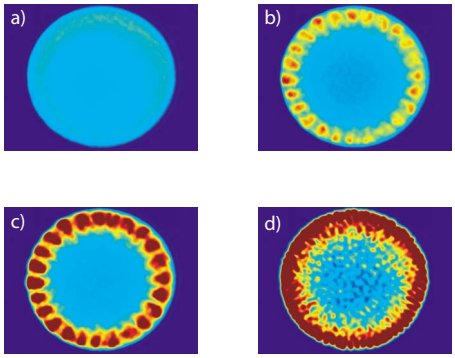

FIG. 2. (Color online) Near field of the total intensity of the solitary VCSEL for different bias currents (a) 11, (b) 12.4, (c) 12.7, and (d) 60 mA.

The output of the VCSEL is monitored either by a charge-coupled device (CCD) camera (Hitachi KP-D50), on which we form an image of the near field or by an optical spectrum analyzer (Ando 6317B) with a resolution of 0.02 nm. A photodiode (Hamamatsu C5331-02) monitors the emission from a portion of the VCSEL transverse plane in order to detect temporal dynamics. The output of this detector is sent to an oscilloscope with a 4 GHz analog bandwidth (Tektronix CSA 7404).

We first study the near-field pattern of the solitary VCSEL for different bias currents (Fig. 2). Due to the current crowding, the laser emission at threshold starts only at the VCSEL periphery with a flower mode profile [Fig. 2(b)]. With increasing bias current, the emission still occurs close to the oxide aperture boundary [Fig. 2(c)] but then it starts filling in all the internal area of the VCSEL aperture, and finally the whole transverse plane is lasing [Fig. 2(d)].

In order to check if the VCSEL is emitting linear polarization in these high-order transverse modes, we measure the light vs current (LI) curves for the principal and the orthogonal polarizations (Fig. 3). As can be seen from this figure, there is a distinct region above the lasing threshold where the

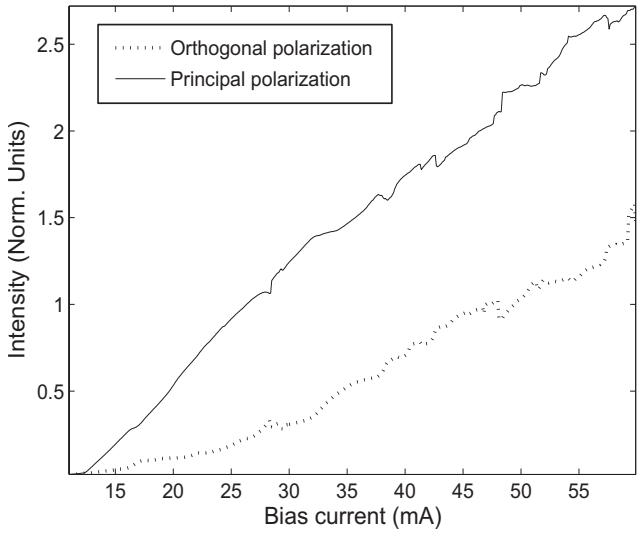

FIG. 3. LI curve for the principal and orthogonal polarizations of the total intensity of the VCSEL.

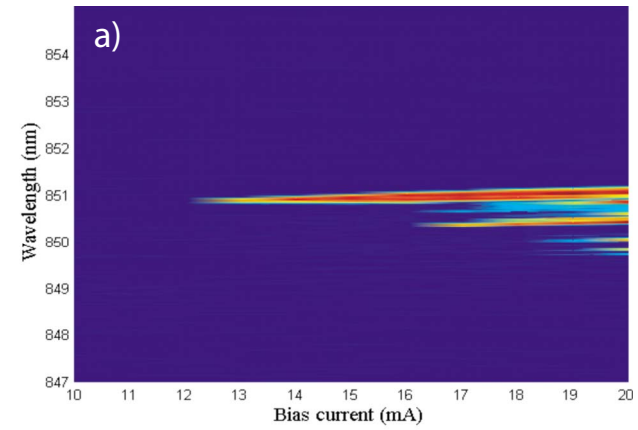

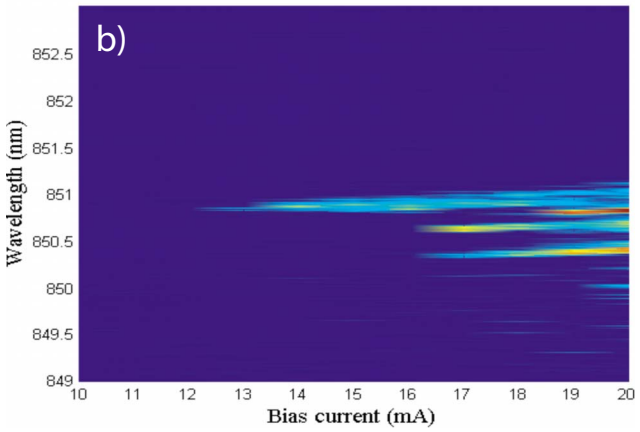

FIG. 4. (Color online) Evolution of the optical spectrum with the injection current for the principal (a) and orthogonal (b) polarization.

VCSEL emission is linearly polarized: the VCSEL starts lasing in the principal polarization at $I \approx 12$ mA, while the threshold of the orthogonal polarization is $I \approx 16$ mA.

The evolution of the optical spectrum for the principal and orthogonal polarizations with the injection current is presented in Figs. 4(a) and 4(b), respectively. As can be seen from this figure, the region of currents for which the VCSEL emits well-defined principal linear polarization coincides with the region of single-wavelength emission, revealing that the flower mode in Figs. 2(b) and 2(c) is actually the only single high-order mode lasing in this current region.

In such a way, if we compare Figs. 2 and 3, we can conclude that the flower mode present in Fig. 2(b) is linearly polarized along the principal direction. This conclusion is further confirmed by Fig. 5, where we show the near-field patterns for principal (x) polarization and orthogonal (y) polarization without (left column) and with (right column) injection of a holding beam with orthogonal (y) polarization. As can be seen from this figure (bottom, left), without a holding beam the flower mode is not present in the near field of the orthogonal polarization, i.e., it is not lasing.

We now make use of the region of injection currents for which the VCSEL is well linearly polarized and introduce a holding beam with orthogonal polarization. Quite interestingly, we obtain a well-pronounced pattern in the orthogonal

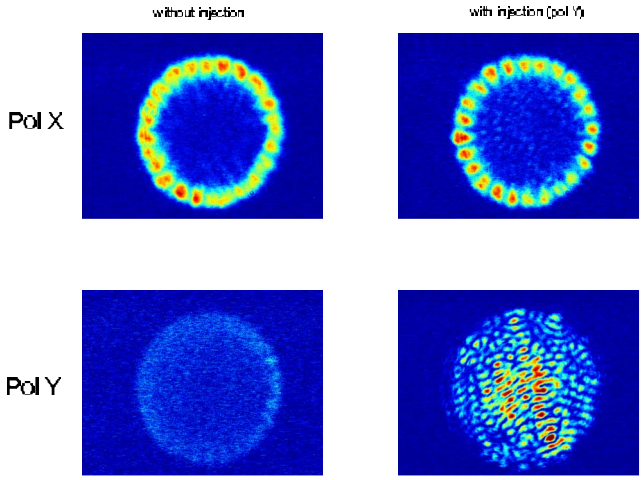

FIG. 5. (Color online) Near field of the VCSEL for principal x and orthogonal y polarizations without (left column) and with (right column) injection of a holding beam with orthogonal polarization. With a holding beam, a pattern in the orthogonal polarization is created in the whole VCSEL area.

polarization near field of the laser [Fig. 5 (bottom, right)] while the VCSEL keeps lasing in the same flower mode for the principal polarization (top, right). The bias current is set to $I=14$ mA and the wavelength and the power of the holding beam are, respectively, 849.51 nm and 8 mW in front of the collimator of the VCSEL.

By changing the wavelength of the holding beam to 851.118 nm and the injection current to $I=16.3$ mA, we are able to create a localized structure in the center of the device [Fig. 6(a)]. This orthogonal polarized localized structure is bistable. Figure 7(a) presents the intensity of a portion of the VCSEL emission beam from the center of the device as a function of the bias current. As can be seen from this figure, the orthogonal polarization localized structure is switched on and off at different currents defining a hysteresis region. Figures 7(b) and 7(c) show the near field of orthogonal polarization at the upper and the lower branch of the hysteresis curve, respectively. We have to stress that it is not possible to obtain such a bistable localized structure in our VCSEL when a holding beam with the principal polarization is injected [see Fig. 6(b)].

In order to support theoretically our experimental findings, we extend the rate equation VCSEL model of [15] for

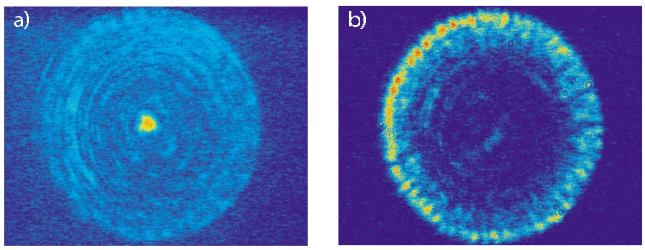

FIG. 6. (Color online) Near field of the VCSEL in orthogonal polarization for two orientations of the linear polarization of the holding beam: (a) orthogonal and (b) principal. In (a) a localized structure in the orthogonal polarization appears in the center of the laser.

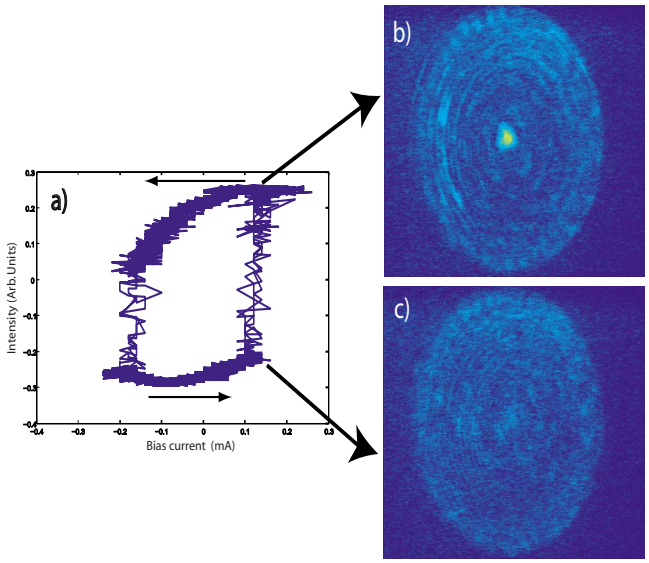

FIG. 7. (Color online) Polarization bistability of the localized structure when the VCSEL injection current is swept forward and backward.

the case of two orthogonal linear polarizations, which are coupled through the carrier density equation. Our model reads

$$\frac{dE_x}{dt} = -(1+\eta_x+j\theta_x)E_x + 2C_x(1-j\alpha_x)(N-1) \times E_x + E_{xi} + j\nabla_\perp^2 E_x, \tag{1}$$

$$\frac{dE_y}{dt} = -(1+\eta_y+j\theta_y)E_y + 2C_y(1-j\alpha_y)(N-1) \times E_y + E_{yi} + j\nabla_\perp^2 E_y, \tag{2}$$

$$\frac{dN}{dt} = -\gamma(N-I+(N-1)|E_x|^2+(N-1)|E_y|^2-d\nabla_\perp^2 N). \tag{3}$$

Here E_x and E_y are the normalized electric fields $E_{x,y}=\sqrt{\epsilon_0 n_{x,y} c\tau_r g_{x,y}/(h\omega_0)}F_{x,y}$ [15], where $F_{x,y}$ are the slowly varying mean field x and y LP components of the electric fields; $n_{x,y}$ are the cavity refractive indices of the x and y LP fields; $g_{x,y}$ are the differential gains; $\alpha_{x,y}$ are the linewidth enhancement factors; and τ_r is the nonradiative carrier recombination time. $\eta_{x,y}=2\alpha_{ix,y}L/T_{x,y}$ with $\alpha_{ix,y}$ the linear absorption coefficients in the regions outside the active layer, L the cavity length, and $T_{x,y}$ the VCSEL mirror transmissivities. $\theta_{x,y}=(\omega_{x,y}-\omega_0)/\kappa_{x,y}$ are the cavity detuning parameters, with $\omega_{x,y}$ the cavity frequencies of the LP fields, ω_0 the frequency of the external field with slowly varying amplitude E_{xi} or E_{yi}, and $\kappa_{x,y}$ the inverse of the photon lifetimes. $C_{x,y}=g_{x,y}L_A N_0/(2T_{x,y})$ with L_A the length of the gain material, N_0 the carrier density at transparency, and $g_{x,y}$ the differential gain coefficients. In the rate equation (3) the carrier density N and current I are normalized to the transparency carrier density N_0 and current I_0; $\gamma=(\kappa\tau_r)^{-1}$ is the nondimensional

decay rate; $d=l_D^2$ with $l_D=\sqrt{D\tau_r}$ the diffusion length and D the diffusion coefficient.

In our model, time is scaled to the photon lifetime (typically, a few picoseconds), while the typical time scale for carrier nonradiative recombination in semiconductors is on the order of 1 ns, in such a way that $\gamma=0.01$ (we take $\gamma=0.1$ during simulations to avoid the long transients). The spatial variables are scaled to the diffraction length $\sqrt{a}$, which in these devices is typically on the order of 4.5 μm [15]. As we expect the experimentally observed behavior to be generic, i.e., not critically dependent on the particular VCSEL, we take the same parameters as in [15]: $C_x=C_y=0.45$, $\gamma=0.1$, $d=0.052$. However, we consider here $\alpha_x=\alpha_y=3$ as typical for VCSELs and different losses $\eta_x=0$ and $\eta_y=0.3$ for the two orthogonal linear polarizations. The detunings for the injected light polarizations are taken to be the same for x and y HBs and are $\theta_x=-0.5$ and $\theta_y=-\alpha(1+\eta_y)$ for the x HB and $\theta_x=-\alpha(1+\eta_x)$ and $\theta_y=-0.5$ for the y HB, respectively. Furthermore, to account for the fact that the VCSEL is of medium size and experiences a strong current crowding, we take a truncated Gaussian-ring profile for the current injection, i.e., $I(r)=0$ for $r>r_a$ and $I(r)=I_0\exp[-(r-r_c)^2/d_r^2]$ for $r\leqslant r_a$ with $r_a=8$, $r_c=7$, and $d_r=8$.

We integrate numerically the dynamical equations using a split-step method with periodic boundary conditions. In Fig. 8 we show the time-averaged light distributions in the principal x polarization [Figs. 8(a) and 8(c)] and in the orthogonal y polarization [Figs. 8(b) and 8(d)] when the holding beam is linearly polarized along the principal polarization [Figs. 8(a) and 8(b)] or along the orthogonal polarization [Figs. 8(c) and 8(d)]. The strength of the holding beam is $E_{yi}=0.4$ and the current is $I_0=2.6$. As can be seen from this figure, we observe qualitatively the same physical picture as in the experiment: a lasing flower mode in the principal x polarization for both x and y polarizations of the holding beam and the appearance in the center of the laser of a localized structure in the orthogonal y polarization when a LP holding beam is applied with the same y polarization. This localized structure is quite robust, e.g., it appears for η_y in the range 0.1–0.3 and also when the detunings of the two LP states are slightly different. Numerical simulations based on a more refined model describing the material polarization dynamics as in Ref. [16], with the inclusion of light polarization, are on the way and will be the subject of a future presentation.

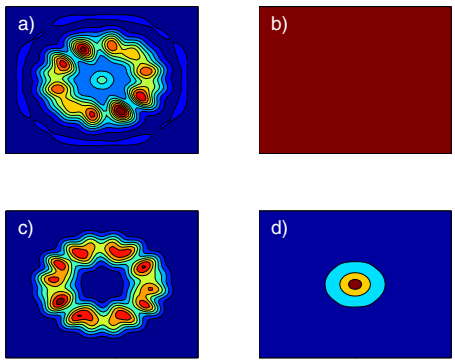

FIG. 8. (Color online) Numerical evidence of localized structure in orthogonal polarization in a medium-size VCSEL. (a), (b) holding beam with a principal x polarization: (a) flower mode in the principal x polarization; (b) no light in the orthogonal y polarization. (c), (d) holding beam with an orthogonal y polarization: (c) flower mode in the principal x polarization; (d) localized structure in the center of the VCSEL for the orthogonal y polarization.

In conclusion, we have provided experimental evidence that medium-size-area VCSELs are capable of supporting spatially localized structures if one makes use of the polarization properties of VCSELs. Such a localized structure with orthogonal polarization has been experimentally demonstrated for a 40 μm GaAs VCSEL biased above the lasing threshold for the principal polarization by injecting a holding beam with orthogonal polarization. Furthermore, the orthogonal polarization localized structure is experimentally shown to be bistable with the injection current. A rate equation model that considers two orthogonal linear polarizations coupled through the carrier density supports the experimental findings when the strong current crowding in the laser is taken into account.

The authors acknowledge the support of Fonds Wetenschappelijk Onderzoek—Vlaanderen, Geconcerteerds Onderzoeksactie, and Onderzoeksraand of Vrije Universiteit Brussel and the European Science Foundation COST 288 action. G.T. also acknowledges the European FET Open Project FunFACS ("Fundamentals, Functionalities, and Applications of Cavity Solitons").

[1] N. N. Rosanov, *Spatial Hysteresis and Optical Patterns* (Springer, Berlin, 2002).
[2] L. A. Lugiato *et al.*, in *Dissipative Solitons: From Optics to Biology and Medicine*, edited by N. Akhmediev and A. Ankiewicz, Lecture Notes in Physics Vol. 751 (Springer, Berlin, 2008).
[3] S. Barland *et al.*, Nature (London) **419**, 699 (2002).
[4] X. Hachair *et al.*, Phys. Rev. A **69**, 043817 (2004).
[5] Y. F. Chen and Y. P. Lan, Phys. Rev. A **65**, 013802 (2001).
[6] F. T. Arecchi *et al.*, Phys. Rev. Lett. **70**, 2277 (1993).
[7] K. D. Choquette *et al.*, IEEE J. Sel. Top. Quantum Electron. **1**, 661 (1995).
[8] K. Panajotov *et al.*, in *Nanoscale Linear and Nonlinear Optics*, edited by M. Bertoletti, C. M. Bowden, and C. Sibilia, AIP Conf. Proc. No. 560 (AIP, Melville, NY, 2001), p. 403.
[9] P. Besnard *et al.*, J. Opt. Soc. Am. B **16**, 1059 (1999).
[10] M. Sciamanna *et al.*, Opt. Lett. **28**, 1543 (2003).
[11] S. Jiang *et al.*, Appl. Phys. Lett. **63**, 3545 (1993).
[12] I. Gatare *et al.*, Phys. Rev. A **76**, 031803(R) (2007).
[13] S. P. Hegarty *et al.*, Phys. Rev. Lett. **82**, 1434 (1999).
[14] N. A. Loiko and I. V. Babushkin, Proc. SPIE **4751**, 382 (2002).
[15] L. Spinelli *et al.*, Phys. Rev. A **58**, 2542 (1998).
[16] X. Hachair *et al.*, IEEE J. Sel. Top. Quantum Electron. **12**, 339 (2006).